Egypt. J. Chem. **Vol. 63,** No. 11 pp. 4659 - 4669 (2020)

Egyptian Journal of Chemistry

http://ejchem.journals.ekb.eg/

Synthesis, Spectroscopic Investigation and Bactericidal Effect of Poly (Vinyl Alcohol) (PVA) - Iron Nanoparticles (Fe Nps)

Afaf Sarhan

Polymer Research Group, Physics Department, Faculty of Science, Mansoura University, Mansoura 35516-Egypt

Abstract

This study aimed to synthesize Poly (vinyl alcohol) - iron nanoparticles (PVA-Fe NPs) via two different methods, the green electrochemical technique in presence of (PVA) which rapid and eco-friendly and by adding different ratios of (Fe-NPs) to PVA, then exposed to different time of UV-irradiation. Characterization of the resulting PVA-Fe NPs was performed using many spectroscopic and analytical techniques such as, UV/Vis spectra, IR Spectroscopy (FT-IR), and X-ray diffraction (XRD). Production of the Fe NPs was verified by appearance of absorbance peaks at about 457 – 462 nm in UV spectra which attributed to surface plasmon resonance. The band gap energy values show decrease with increasing Fe NPs. FTIR spectra confirm the interaction between PVA polymer and Fe- nanoparticle. All the developed PVA-Fe NPs displayed antibacterial efficiency against both Staphylococcus aureus and Escherichia coli bacteria. Moreover, the antibacterial efficiency enhanced by increasing Fe content and UV irradiation time.

Keywords: Antibacterial activity; Band gap; Electrochemical method; Fe nanoparticles; PVA.

Introduction

The science of nanotechnology is a branch of science that focuses on the manipulation of atoms and molecules in the nanometer size range (mostly, 100 nm or less) [1-8]. Nanoparticles (NPs) become a remarkable in the research field of textiles and fibers [9], forensic science [10], electronics [11], space [12], agriculture [13, 14], and mainly in medical applications, because they involve the capability to deliver a vast range of drugs to altering the body areas for fixed interval of time. The size ranges for NPs from 1 nm to 1000 nm.

Nanoparticles are solid colloidal particles construct of natural, synthetic, or semi-synthetic polymers [15]. Recently, the studies opened under green chemistry for the search of goodly methods for the perfection NPs, searching antioxidant, antibacterial, and anti-cancer activity of natural molecules [16-20]. Generally, the superior metal- nanoparticles were produced utilizing various tools involve (a) a reduction of metal with the assist of ($NaBH_4$), ascorbate and citrate acts as a reducing agent [2, 6, 21] (b) the ir-radiation of the solution contain metal ions for ultraviolet and visible light [22], or against ultrasound irradiation and microwave [23-28] (c) bio-organisms and bio-molecules, such as, polysaccharides, bacteria and proteins have been also used successively for the synthesis of the grand metal nanoparticles mainly Ag and gold nanoparticles [29-33].

Fe is the fourth most abundant element in the earth`s crust, and is very important in the biosphere. Waste effluents from steel tempering, coal coking, mining industries and so on, contain large quantities of Fe, and excessive Fe ions in water will pollute the environment [34]. Iron is important for most living organisms due to it is required for many metabolic processes including oxygen transport, drug metabolism, DNA synthesis, ATP production, steroid synthesis and electron transport [35]. An electrochemical mechanism was used for the first time for the

*Corresponding author e-mail: afaf_sarhan2003@yahoo.com
Receive Date: 04 July 2020, Revise Date: 19 August 2020, Accept Date: 25 August 2020
DOI: 10.21608/EJCHEM.2020.34685.2725

synthesis of nanoparticles by Helbig and Reetz [36]. In the equipping, the sheet of metal was liquefied and then the obtained metal -ions were decreased in the cathode, producing metallic particles stabled via tetra alkyl ammonium salts. The major properties of the electrochemical mechanism involve the large rarity of the resulting nanoparticles (NPs) and the resistance of size particle rule by setting the current density even required to vacuum equipment. Since then, this approach has been adopted for the fabrication of plethora of metal NPs. D. Gopi et al. [37], synthesized uniform iron nanoparticles with very fine size (ranged from 21 to 9 nm) utilizing electrochemical approach. This has been achieved via electro-oxidation of iron in the presence of ferrous perlocate as an aqueous medium. Alghazade *et.al.* [38], prepared ultra-fine Fe-NPs for supercapacitors application. Fe-NPs prepared by employing simple electro-synthesis approach with the aid of PVA as an assisted electrolyte. The resultant NPs have small average size about 15nm. The obtained results declared that PVA acts as coating for the prepared NPs and hence prevent them from aggregation or agglomeration.

Poly (vinyl alcohol) PVA, is a semi crystalline polymer [39], and is a widely used synthetic polymer. The benefit of its use lies in its properties: non-toxicity, water-solubility, bio-compatibility, bio-degradability and excellent mechanical properties, and have many interesting physical properties, which arise from the presence of OH groups and the hydrogen bond formation [40-45]. The orderly linear structure of Poly (vinyl alcohol) for a vast number of side (OH) groups on the main chain proposes superior reactivity and hydrophilicity. In addition, its low price and wide availability makes PVA a polymer of choice in a large number of applications. PVA is a potential material having high dielectric strength and good charge storage capacity and dopant-dependent electrical and optical properties. It has carbon chain backbone with hydroxyl groups (OH) attached to methane carbons. These OH groups can be a source of hydrogen bonding and hence assist the formation of polymer composite [46].

Due to the above reasons the main goal of the this work was devoted to the fabrication and characterization of a soluble PVA-Fe NPs by two different methods, the first one is green synthesis of PVA-Fe by electrochemical method and the second method by adding Fe NPs to PVA polymer, also to study the influence of UV-irradiation reduction to Poly (vinyl alcohol) -iron nanoparticle. Additionally, evaluate the activity of antibacterial of PVA-Fe nanoparticles before and next subjected to the reduction of UV. The prepared nanoparticles were described by UV analysis, FT-IR and X-ray diffraction pattern. The band gap was also calculated from UV spectroscopy.

Materials and methods

Materials

PVA (M_w=72,000) is purchased from Merck, (Germany) and iron plate of purity 99.99%, were purchased from Sigma–Aldrich (St. Louis, USA). The iron plate was well polished before use with the assist of a very fine emery paper, cleaned by ethanol, acetone (90%) and de-ionized water and used as anode. Platinum sheet acquired from Sigma, was well scoured before used as cathode. Iron Powder (Fe, 99.9 %, 800 nm), Stock#: US1034M, CAS#:7439-89-6, Net weight: 500 g (USA).

Deionized water was used for all sample preparation.

Methods

PVA is prepared by dissolving in deionized water and continuously stirred using a hot plate with magnetic stirrer to embed homogeneous mixture. The PVA/Fe complexes were constructed from the electrochemical method and then exposure to UV-irradiation for different times. This process was achieved utilizing a potentiostatic method at 2 V. The cell included of Fe plate working as anode and Pt plates as cathode. These 2 electrodes were submersed perpendicular in the electrolytic solution. The electrical contact was made connected to a convenient changed resistor, Picometer (Keithly 485), voltmeter (Keithly175) and potential power supply (ECOS). The solution was equipped by dissolving 1wt% of PVA into de-ionized water with the aid of stirrer to complete dissolving and to eliminate any burst. This process was achieved for various periods (8, 24, and 60) h. Finally, centrifuge the solution at 4000 rpm till 600 sec, then infiltered to eliminate all traces in the solution. Next, the resulting PVA/Fe solution exposed to UV-irradiation by UV- lamp with λ_{max} = 254 nm at about 25 °C (1&2& 3) h. The solution is then casted in petri dish and dried in an oven at T = 50 ° C for one week.

Doped PVA samples with different ratio of Fe NPs are prepared by dissolving them in de-ionized water at T = 333 K for 24 h. The solution is continuously stirred using magnetic stirrer to

ensure homogeneous mixture. The solution is then casted in petri dish and dried in an oven at T=333 K for 24 h.

Instrumental analyses

The UV-Visible spectra of the PVA-Fe samples were obtained in the range of 200-800 nm using ATI Unicom UV-Vis spectrophotometer with UV-Vis vision software V 3.20. The analysis was performed at room temperature using quartz cuvettes (1 cm optical path. Mattson 5000 FTIR spectrometer was recorded at 25 °C from 400–4000 cm^{-1} at (8 cm^{-1}) of resolution. The drop of lightened PVA-Fe solvent was diffused in the planar freshly NaCl disks. The solution was entirely forced further T= 323°K. Next, the disks were set in the holder of the sample of the spectrometer. X-ray diffraction pattern of all samples is record using Rigaku Ultima IV diffractometer with Cu–Kα radiation (λ= 1.5418 *A*º) at 40 kV. Also, the degree of crystallinity of the improved samples was determined by using the Material Studio Vision software with version 7.

Antibacterial efficiency

The efficiency of antibacterial of the pure PVA and PVA- Fe NPs with various iron ratio before and after of exposure to UV irradiation with different time intervals (1, 2 and 3) h was evaluated versus "Staphylococcus aureus (S.aureus) and Escherichia coli (E. coli)" with agar well- diffusion procedure. One ml of bacterial cell suspension (10 CFU/ml) was inoculated on Muller – Hinton Agar medium. Four wells were made with sterilized 5 mm cork borer, the different ratios were poured into the wells. The plates were remained at room temperature for 2 h to allow the test sample diffusion, then incubated face upwards at 37 º C for 24 h. All experiments were occurred in duplicate and mean values were presented. The antibacterial efficiency was investigated by measuring the diameter of the clear zone around every well [47].

Results and discussion

UV/visible spectroscopy

The UV-Vis spectra of, are shown in Fig.1. It is clear that PVA-Fe complexes has UV-Vis spectra various to that of pure PVA. PVA spectra shows absorbance band at 275 nm. This peak is red shifted to 357 nm, and the absorbance intensity increase with increasing electrolytic time (8, 24, 60) h. Further increase in electrolytic time (8, 24 and 60) h leads to the appearance of new absorption bands around (457 – 462) nm that associated with Fe which indicates to the plasmon-resonance of Fe nanoparticles and indicated to the formation of nanoparticles [48]. Additionally, this peak is accountable for the convert color from yellow to brownish for the prepared NPs, where the color of the samples was varied from transparent to pinkish red. Additionally, it is found increase in peak intensity and a slight shift in peak position can be noted with increasing the complexation time. This perception characterized the complexation of Fe/NPs via functional group of PVA.

Fig.2 showed the effect of UV- irradiation time on PVA-Fe NPs. It is found that, increasing the irradiation time for 60 h leads to significant excess in the peak and show a slight increase in the peak intensity from (453-493) nm as compared to 8 h. Further increasing in UV irradiation time at 60h-for 3h results in significant decrease in intensity of first peak and vanishing of the second one due to scission and fragmentation in the polymer chain [47].

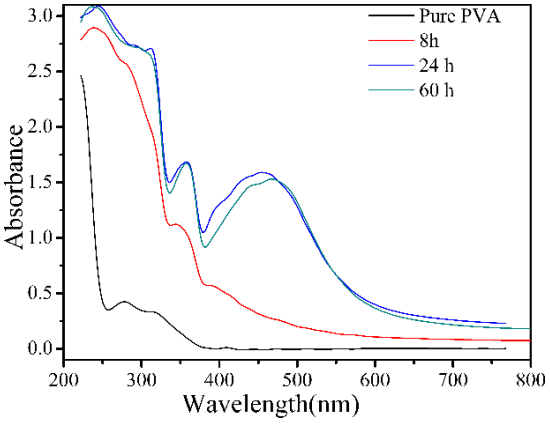

Fig.1. UV-Vis spectra of pure PVA and PVA-Fe NPs with different electrolytic time.

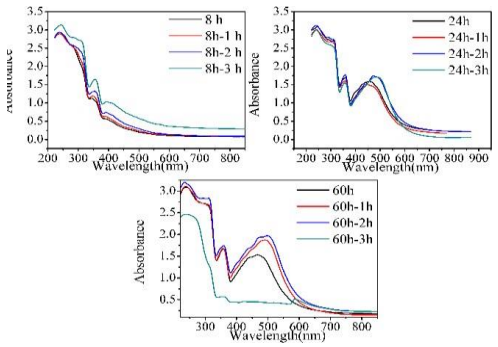

Fig.2. UV- spectra of the PVA-Fe NPs obtaining by electrochemical method for different times (8, 24 and 60) h then exposed to UV-irradiation for various intervals (1, 2and 3) h.

Fig.3. displays the UV-Vis spectra of PVA and PVA-Fe NPs samples with different ratio of Fe NPs (0.01, 0.05 and 0.1). These samples show strong absorbance band at 426 shifted to 460 nm and the absorbance peak gradually increases with increasing Fe NPs content. These peaks assigned to the surface plasmon resonance which confirm the existence of Fe NPs within PVA polymer. This red shift implies the increase of Fe NPs size. There is no peak appeared at higher ratio (0.1) due to scission and fragmentation in the polymer chain.

Fig.4 showed the effect of UV- irradiation time on PVA-Fe NPs. It is found that, increasing the irradiation time leads to significant enhance in the peak and show a slight increase in the peak intensity.

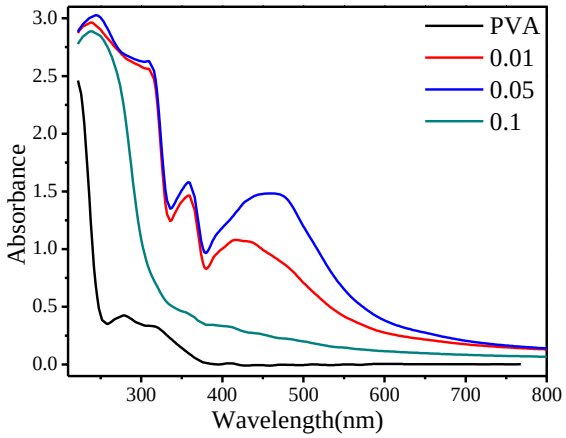

Fig.3. UV-Vis spectra of the PVA-Fe NPs with different ratio of Fe NPs.

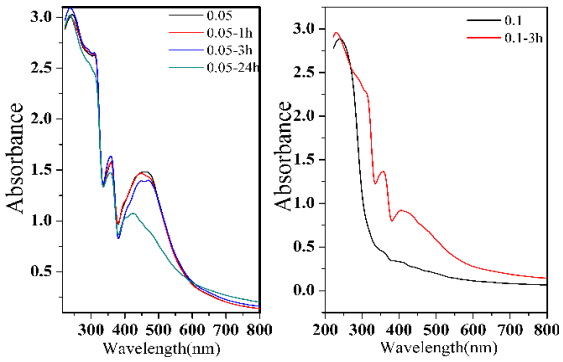

Fig.4. UV- spectra of the PVA-Fe NPs for different ratios (0.05 and 0.1) Fe NPs followed by exposing to UV-irradiation for various periods (1& 3 and 24) h.

Calculation of the Energy band gap E_g

Also, the surface plasmon resonance verify the change in optical-energy E_g of the PVA-Fe NPs samples. The E_g rates of PVA-Fe NPs is deduced by Tauc's relation and supplied by Davis and Mott [49]:

$$\alpha hu = (\alpha hu - E_g)^n$$

where (hu) is the photon energy, h is plank`s constant, u is the frequency, A is a constant, n is equal 1/2 for direct band gap and the absorption coefficient (α) obtained by the relation [50]:

$$\alpha = 4\pi K/\lambda$$

where k is the absorption index or absorbance and λ the wavelength. Plotting the relationship between $(\alpha hu)^2$ versus the photon energy (hu) show straight portion, band gap can be calculated by extrapolating this straight portion $[(\alpha hu) = 0]$ as shown in Fig.(5 & 6) and Table (1&S1 (see Electronic Supplementary Material Table S1)).

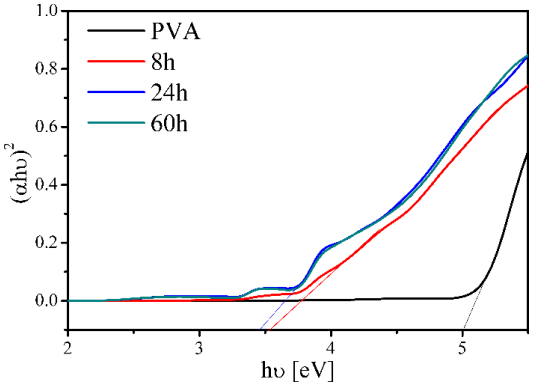

Fig.5. The relation between (αhν)2 via the photon energy (hν) of PVA and (PVA-Fe NPs) with different electrolytic time.

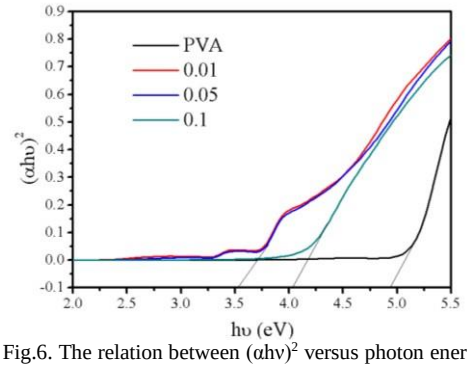

Fig.6. The relation between $(\alpha h\upsilon)^2$ versus photon energy ($h\upsilon$) of the PVA-Fe NPs with different ratio of Fe NPs.

$(\alpha h\upsilon)^2$ on photon energy axis, as manifested in Fig.(5&6), and listed in Table (1& S1 (see Electronic Supplementary Material Table S1)). The estimated values of allowed direct band gap energy PVA-Fe samples before and after exposure to UV- irradiation show a remarkable decrease in band gap in different concentrations as compared to pure PVA indicating an improving the structure of pure PVA. It is clear that, with increasing UV-irradiation time, a slightly change in the energy gap is decreased. Therefore, the conductivity will enhance, resulting in a decreasing in optical energy gap.

Table 1. The values of direct band gap energy of pure PVA and PVA-Fe NPs with different electrolytic time before and after irradiation.

	Direct energy gap, (eV)			
Sample	Before UV-irradiation	After 1 h irradiation	After 2 h irradiation	After 3 h irradiation
Pure PVA	4.954	-	-	-
8 h	3.543	3.429	3.387	3.370
24 h	3.43	3.364	3.373	3.375
60 h	3.341	3.3492	3.376	3.420

3.2. FTIR investigation

Due to its capability to detect the existence of molecular interactions and structural alterations, FTIR spectroscopy has been used to investigate the PVA-Fe NPs complexes and nanocomposites. Fig.7 depicts the FTIR spectra of PVA-Fe NPs with different electrochemical time comparing with the neat of PVA. The spectra of PVA is characterized by various absorption bands at certain wavenumbers, such as, the absorption band at 848 cm^{-1} which is corresponds to CH_2 rocking vibration [51]. The bands at 914 cm^{-1} and 1095 cm^{-1} can be correlated to the CO Symmetric Stretching [52] and to C–O stretching motion of acetyl groups exist on the PVA backbone [53], while the bands at about 1334 cm^{-1} and 1432 cm^{-1} is attributed to CH_2 out of plane bending and OH and C-H bending-vibration. The band at 1565 cm^{-1} corresponds to NHCO and vibrational band at 1655 cm^{-1} which assigned to C=C stretching of PVA [54]. Also, the IR peak at 1721 cm^{-1} is assigned to stretching (C=O) and (C-O) from acetate group keeping from pure PVA, a peak at 2932 indicates to the CH_2 asymmetric stretching and bands in the range from 3237 to 3400 cm^{-1} are assigned to (OH) intermolecular hydrogen bonded [55].

The FTIR analysis of the PVA-Fe complexes, produced at various oxidation times, display many changes from that of PVA. For example, the *bands in* the range from 3237 to 3400 cm^{-1} which assigned to (OH) intermolecular hydrogen bonded of PVA with Fe-NPs [56]. The other bands of PVA nearly kept their location in the conforming PVA-Fe complexes, but with a variation in their intensity. A similar behavior was also noted in the case of PVA-Fe samples obtained. The FT-IR spectra of the PVA-Fe complexes are located completely changed in comparison to that of the PVA, where some vibrational bands are changed.

The absorbance of the functional bands in the wavenumber range 1565 cm^{-1} and 1721 cm^{-1} increases gradually with the increase of electrolytic time. The distinctive bands of PVA is remarkably shifted to new wavenumbers or even completely vanished which represents a clear evidence of chemical interactions bonding between PVA and Fe NPs. The characteristic band of PVA at 1095 cm^{-1} indicated to C-O stretching motion is reduced and split and appear new band at 1130 for 24 and 60 h. Thus, these considerable alterations in the absorbance of all bands refer to exist the production of nanoparticle-polymer interactions. This performs to a reduction in the degree of crystallinity of the nanoparticle samples and also, the formation of complexes. FTIR analysis of the PVA-Fe films exposed to UV- irradiation shown in Fig. S1 (see Electronic Supplementary Material Fig)

demonstrated slightly considerable variation from the corresponding spectra before-UV- irradiation, where some vibrational bands are changed and it further verify the complete complexation between PVA groups with Fe. The absorbance of the functional bands in the wavenumber range 1710 cm^{-1} for 24 h disappeared and band at 841 cm^{-1} increases gradually with exposed time.

Fig.(8&9) illustrate the spectra of PVA and PVA-Fe NPs with different ratio of Fe NPs and the spectra of PVA and PVA-Fe NPs for different ratios (0.05 and 0.1) Fe NPs followed by exposing to the reduction for various intervals (1& 3 and 24) h. The FT-IR spectra of the samples (0.05 and 0.1 wt.% Fe NPs) are found varied in comparison to that of the pure PVA such as the band at 3330 is shifted and increases gradually. Thus, these consider-able alterations in the absorbance of all bands refer to exist the production of nanoparticle-polymer interactions, such hydrogen bonding through the groups [(OH) / (COO−)] of PVA and Fe NPs [52].

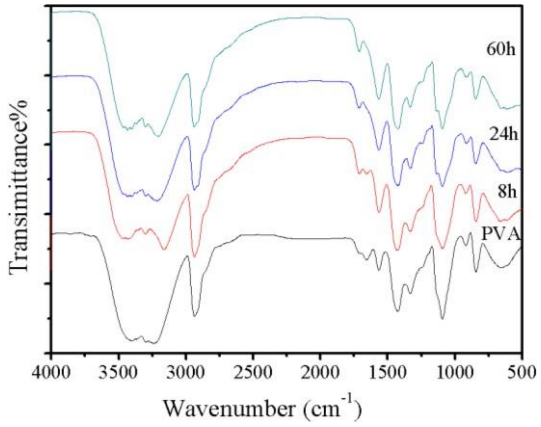

Fig.7. The spectra of PVA and PVA-Fe NPs after different times of complexations**.**

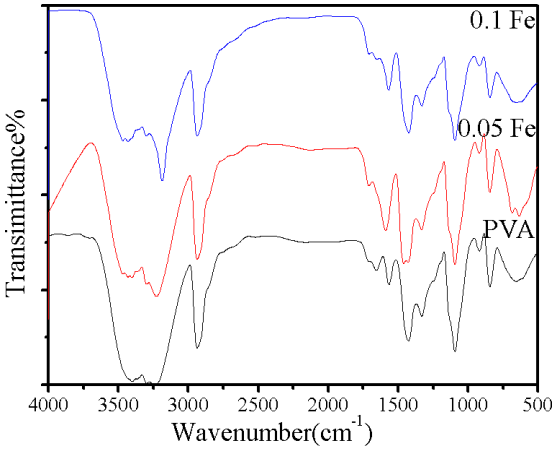

Fig.8. The spectra of PVA and PVA-Fe NPs with different ratio of Fe NPs.

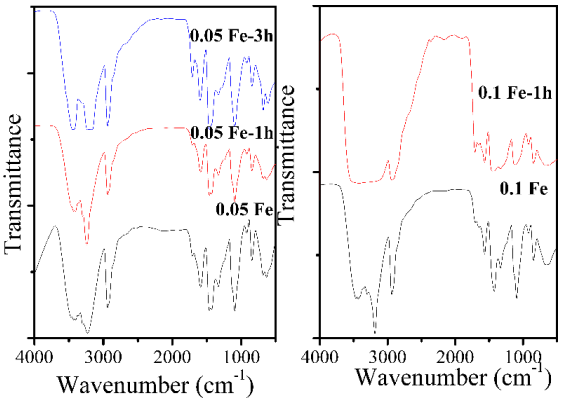

Fig.9. The spectra of PVA and PVA-Fe NPs for different ratios (0.05 and 0.1) Fe NPs followed by exposing to UV- reduction for various periods (1& 3 and 24) h.

X-ray diffraction test

The crystallographic patterns of pure PVA and PVA/Fe complexes resulting at various electrolysis time (8, 24 and 60) h illustrated in the Fig.10. As seen of the Figure, the semi-crystalline PVA polymer is characterized by two sharp reflection bands at $2\theta^{o}$ = 10.8^{o} and 19.7^{o} respectively, the result indicating that, main peak at 2θ=19.7° is refer to the crystalline structure of PVA that refers to orthorhombic PVA (101) reflection plane [52]. While, the XRD pattern of PVA/Fe complexes, no peaks of Fe nanoparticles were appeared in XRD test of the complexes, which indicated the complete dissolution of Fe nanoparticles in the polymer matrices. The XRD studies confirmed the fact that there exists a specific complex between PVA and Fe nanoparticles [57].

The mechanism of ionic transport in polymer electrolytes is still not completely understood, but there is a significant motion of polymer chains existing in the amorphous domain or phase while non-conducting in the crystalline phase. The XRD analysis of PVA solid polymer electrolyte film appears a broad peak which is correlated with the amorphous domain of PVA polymer matrix. The PVA matrix combined with Fe has a larger domain of amorphous phase, so the ionic conductivity of polymer electrolyte can be significantly enhanced [58].

To obtain the information on the crystal structure, X-ray diffraction patterns of pure PVA and PVA/Fe complexes resulting at various electrolysis time (8, 24 and 60) h and then subjected to the reduction for (1 and 3) h were displayed in Fig.11. In the diffractograms of the PVA/Fe samples, it observed that, the peak intensity at 2θ=19.7° is decreases by increasing the electrolysis time and slightly shifted.

The XRD - analysis have been entire for the PVA films and the synthesized Fe nanoparticles at different ratio (0.01, 0.05 and 0.1), displayed in Fig.12, to screened the variation within the structure of the PVA Fe/NPs samples. It is noticed that, the peak intensity was reduced by the cooperation of nanoparticles within the matrix of PVA. Furthermore, no exist diffraction peaks assigned to NPs phases, which refers to the solution of nanoparticles in the matrix [59, 60]. The perceptions describe that, the interactions of NPs-polymer weak the crystallites of PVA and reduces the crystalline phases of the NPs samples. Also, the crystalline phases of PVA were disturbed into the samples due to the interaction of Fe NPs with the PVA chain. The reduction of (Xc%) is significant to the development of the conductivity [52].

Degree of crystallinity (Xc%) for the PVA-Fe NPs at various times of complexations and with different ratio of Fe NPs are shown in Fig.13 (a&b) and Table (S3&S4 (see Electronic Supplementary Material Tables S3&S4)). The (Xc%) reduce with increasing the Fe NPs ratio in the matrix of PVA.

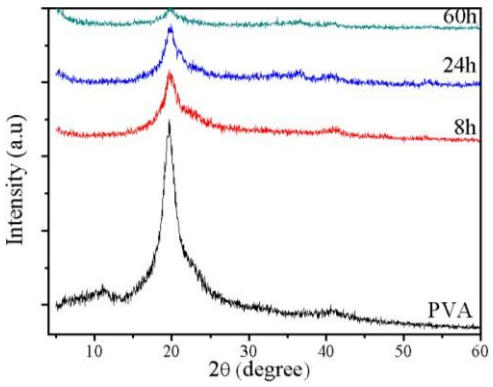

Fig.10. XRD test of virgin PVA and PVA-Fe NPs at different times of complexations (8, 24 and 60) h.

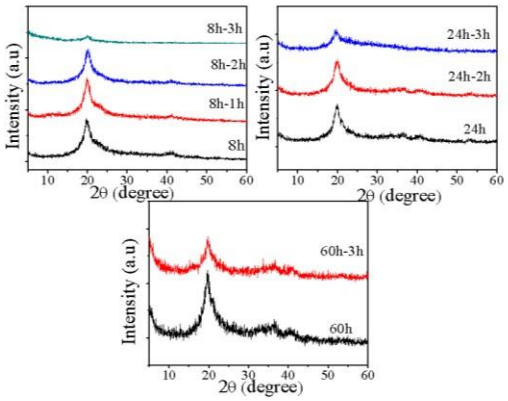

Fig.11. XRD analysis of PVA-Fe NPs at various times of complexations (8, 24 and 60) h after exposure to UV- reduction for various times (1&2 and 3) h.

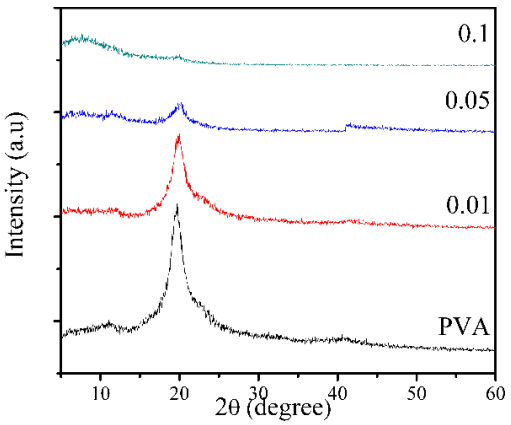

Fig.12. XRD patterns of pure PVA and PVA-Fe NPs with different ratio of Fe NPs.

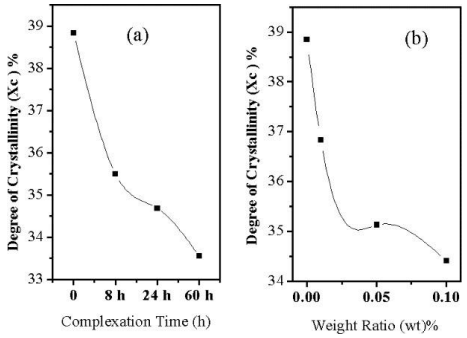

Fig.13: Degree of crystallinity (Xc%) for the PVA-Fe NPs (a) at various times of complexations and (b) with different ratio of Fe NPs**.**

Antibacterial efficiency of PVA-Fe NPs

The antibacterial activity of PVA-Fe nanoparticles and its virgin component have been assigned via Gram-positive (S.aureus) and Gram-negative (E. coli) bacteria, as illustrative examples showed in Fig.14. The acquired data illustrated that every samples exhibit antibacterial activity via both (Staphylococcus aureus) and (Escherichia coli) with different inhibition zone as depicted in the (Table S5 (see Electronic Supplementary Material Table S5)). PVA-Fe nanoparticles shows higher antibacterial activity compared to PVA not appeared. It is worth noting that PVA-Fe NPs exhibited enhanced antibacterial activity with increasing Fe ratio. This effect could be ascribed to the high surface area and the size of the developed nanoparticles, which facilitates their interactions with important components of bacterial cell such as protein and DNA which in turn results in bacterial cell death. Moreover, the production of reactive oxygen species by Fe-NPs could be regarded as proposed mechanism for their antibacterial activity [61].

The inhibition zones of PVA-Fe NPs with a different weight ratio of Fe nanoparticles display increasing with increasing Fe weight ratio revealing an enhancement in antibacterial activity. UV irradiation displays an effect

on antibacterial activity as shown in Table 6. It can be noted from inhibition zone values, increasing of exposure time of UV irradiation lead to enhancement in antibacterial activity of nanoparticles in all weight ratio and against both (Staphylococcus aureus) and (Escherichia coli). But it is worth to mention that, in general, nanoparticles irradiated for (3 h) shows the highest inhibition zone that may be due to the assumption that degradation occurs in polymer backbone which in turn release more ion into the media [62].

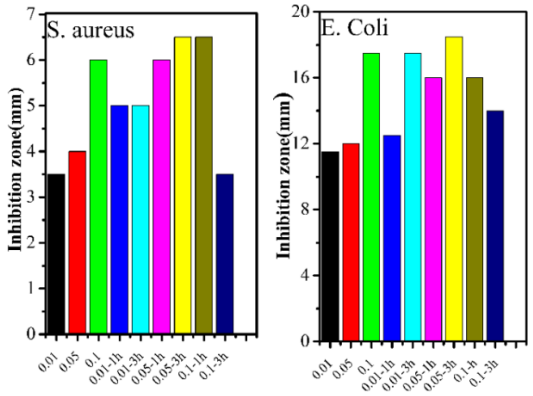

Fig.14: The inhibition zones produced before and after UV-irradiation from PVA and the PVA-Fe NPs improved at various times (1 &3) h.

Conclusions

The iron nanoparticles composed of PVA Fe NPs matrix has been prepared by two methods, the first method the green synthesis of iron nanoparticles by using the electrochemical method and the second method with different concentration of Fe NPs as nanofiller to PVA matrix by casting technique. The characterizations were achieved to assign the functional groups, crystalline structure and surface plasmon resonance of the improved PVA-Fe NPs. The spectra of UV described the production of Fe NPs with the PVA samples from the existence of Surface plasmon resonance of Fe NPs around 420 nm. There is no peak appeared at higher ratio (0.1) due to scission and fragmentation in the polymer chain. Additionally, the UV spectra appeared the reduction of E_g rates obtained from the plot of $(\alpha h\nu)^2$ against photon energy ($h\nu$) with increasing the Fe content. FT–IR analysis manifested the interaction and the complexation between PVA polymer and Fe NPs occurred. X-ray results, indicated to the PVA sample is semi-crystalline, also the (Xc %) was decreased by the combination of Fe NPs. Moreover, polymer matrix such PVA is also known for its biocompatible nature and favorable for biomedical applications. Hence, this method can be quite applicable as a wound healing material, in sensing or other biomedical uses. Studies with S. aureus and E. coli revealed higher influence of Fe NPs with UV-irradiation. The enhanced PVA-Fe NPS also demonstrated a higher antibacterial activity against Gram-positive Staphylococcus aureus (S.aureus) and Gram-negative Escherichia coli (E. coli) bacteria by comparing with that of the control (PVA) and the efficiency of antibacterial enhanced upon enhancing concentration. These results offer that, prepared NPs used in many applications.

Conflicts of interest

The authors declare no conflicts of interest regarding the publication of this paper.

Acknowledgments

The authors much gratefully to Prof. M. T. Ahmed, Prof. T. Fahmy department of physics, Faculty of Science, Mansoura University, Egypt, for supporting me.

References

[1] Dahanayaka D.H., Wang J.X, Hossain S., Bumm L.A., Optically transparent Au {111} substrates: Flat gold nanoparticle platforms for high-resolution scanning tunneling microscopy. Journal of the American Chemical Society, 128 (18), 6052- 6053 (2006)

[2] Ding S., Qian W., Tan Y., Wang Y., In-situ incorporation of gold nanoparticles of desired sizes into three-dimensional macroporous matrixes. *Langmuir*, **22** (17), 7105-7108 (2006).

[3] Larsson M., Lu J., Lindgren J., Surface-enhanced Raman scattering from analytes adsorbed on gold nanoparticles inside polymer beads. *Journal of Raman Spectroscopy*, **35** (10), 826- 834 (2004).

[4] Lu S., Gao W., Gu H.Y., Construction, application and biosafety of silver nanocrystalline chitosan wound dressing. *Burns*. **34**(5), 623-628 (2008).

[5] Ni W., Chen H., Kou X., Yeung M.H., Wang J., Optical fiber-excited surface plasmon resonance spectroscopy of single and ensemble gold nanorods. *The Journal of Physical Chemistry C*. **112** (22), 8105-8109 (2008).

[6] Tan Y., Qian W., Ding S., Wang Y., Gold-nanoparticle-infiltrated polystyrene inverse opals :a three-dimensional platform for generating combined optical properties. *Chemistry of materials*. **18** (15), 3385-3389 (2006).

[7] Wakayama H., Setoyama N., Fukushima Y., Size-Controlled Synthesis and Catalytic Performance of Pt Nanoparticles in Micro-and Mesoporous Silica Prepared Using Supercritical Solvents. *Advanced Materials*. **15** (9), 742-745 (2003).

[8] Xiong Y., McLellan J.M., Chen J., Yin Y., Li Z-Y, Xia Y., Kinetically controlled synthesis of triangular and hexagonal nanoplates of

palladium and their SPR/SERS properties. *Journal of the American Chemical Society*. **127**(48), 17118-17127 (2005).

.

[9] Perelshtein I., Applerot G., Perkas N., Guibert G., Mikhailov S., Gedanken A., Sonochemical coating of silver nanoparticles on textile fabrics (nylon, polyester and cotton) and their antibacterial activity. *Nanotechnology*. **19** (24), 245705 (2008).

[10] Choi M.J., McDonagh A.M., Maynard P., Roux C., Metal-containing nanoparticles and nano-structured particles in fingermark detection. *Forensic science international*. **179** (2-3), 87-97 (2008).

[11] Huang D., Liao F., Molesa S., Redinger D., Subramanian V., Plastic-compatible low resistance printable gold nanoparticle conductors for flexible electronics. *Journal of the electrochemical society*. **150** (7), G412-G417 (2005).

[12] Liu T.M., Musinski L.D., Patel P.R., Gallimore A.D., Gilchrist B.E., Keidar M., Nanoparticle electric propulsion for space exploration. *AIP conference proceedings*: *American Institute of Physics*, **880**, 787-794 (2007).

[13] Speiser B., Nano-particles in organic production? Issues and opinions, 2008.

[14] Lai F., Wissing S.A., Müller R.H., Fadda A.M., Artemisia arborescens L essential oil-loaded solid lipid nanoparticles for potential agricultural application: preparation and characterization. *Aaps Pharmscitech*. **7** (1), E10 (2006).

[15] Wilson B., Samanta M.K., Santhi K., Kumar K.S., Ramasamy M., Suresh B., Chitosan nanoparticles as a new delivery system for the anti-Alzheimer drug tacrine. *Nanomedicine: Nanotechnology, Biology and Medicine*. **6** (1), 144-152 (2010).

[16] Parashar V., Parashar R., Sharma B., Pandey A.C., Parthenium leaf extract mediated synthesis of silver nanoparticles: a novel approach towards weed utilization. *Digest Journal of Nanomaterials & Biostructures (DJNB)*. **4** (1), 45-50 (2009).

[17] Philip D., Biosynthesis of Au, Ag and Au–Ag nanoparticles using edible mushroom extract. *Spectrochimica Acta Part A: Molecular and Biomolecular Spectroscopy*. **73** (2), 374-381(2009).

[18] Smitha S., Philip D., Gopchandran K., Green synthesis of gold nanoparticles using Cinnamomum zeylanicum leaf broth. *Spectrochimica Acta Part A: Molecular and Biomolecular Spectroscopy*. **74** (3), 735-739 (2009).

[19] Song J.Y., Jang H-K, Kim B.S., Biological synthesis of gold nanoparticles using Magnolia kobus and Diopyros kaki leaf extracts. *Process Biochemistry*. **44** (10), 1133-1138 (2009).

[20] Thakkar K.N., Mhatre S.S., Parikh R.Y., Biological synthesis of metallic nanoparticles. *Nanomedicine: nanotechnology, biology and medicine*. **6** (2), 257-262 (2010).

[21] Setua P., Chakraborty A., Seth D., Bhatta M.U., Satyam P., Sarkar N., Synthesis, optical properties, and surface enhanced Raman scattering of silver nanoparticles in nonaqueous methanol reverse micelles. *The Journal of Physical Chemistry C*. **111**(10), 3901-3907 (2007).

[22] Ghosh S.K., Kundu S., Pal T., Evolution, dissolution and reversible generation of gold and silver nanoclusters in micelle by UV-activation. *Bulletin of Materials Science*. **25** (6), 581-582 (2002).

[23] Rocha T.C., Winnischofer H., Westphal E., Zanchet D., Formation kinetics of silver triangular nanoplates. *The Journal of Physical Chemistry C*. **111** (7), 2885-2891 (2007).

[24] Wei D., Qian W., Chitosan-mediated synthesis of gold nanoparticles by UV photoactivation and their characterization. *Journal of nanoscience and nanotechnology*. **6**(8), 2508-2514 (2006).

[25] Callegari A., Tonti D., Chergui M., Photochemically grown silver nanoparticles with wavelength-controlled size and shape. *Nano Letters*. **3** (11), 1565-1568 (2003).

[26] Kurihara K., Kizling J., Stenius P., Fendler J.H., Laser and pulse radiolytically induced colloidal gold formation in water and in water-in-oil microemulsions. *Journal of the American Chemical Society*. **105**(9) 2574-2579 (1983).

[27] Mallikarjuna N.N., Varma R.S., Microwave-assisted shape-controlled bulk synthesis of noble nanocrystals and their catalytic properties. *Crystal growth & design*. **7** (4), 686-690 (2007).

[28] Chiu T-C., Chiou S-H., Hsieh M-M., Chen Y-T., Chang H-T., Photosynthesis of gold nanoparticles in presence of proteins. *Journal of nanoscience and nanotechnology*. **5** (12), 2128-2132 (2005).

[29] Shankar S.S., Rai A., Ankamwar B., Singh A., Ahmad A., Sastry M., Biological synthesis of

triangular gold nanoprisms. *Nature materials*. **3**(7), 482-488 (2004).

[30] Bhainsa K.C., D'souza S., Extracellular biosynthesis of silver nanoparticles using the fungus Aspergillus fumigatus. *Colloids and surfaces B: Biointerfaces*. **47** (2), 160-164 (2006).

[31] Chandran S.P., Chaudhary M., Pasricha R., Ahmad A., Sastry M., Synthesis of gold nanotriangles and silver nanoparticles using Aloevera plant extract. *Biotechnology progress*. **22**(2), 577-583 (2006).

[32] Willner I., Baron R., Willner B., Growing metal nanoparticles by enzymes. *Advanced Materials*, **18** (9), 1109-1120 (2006).

[33] Lengke M.F., Fleet M.E., Southam G., Biosynthesis of silver nanoparticles by filamentous cyanobacteria from a silver (I) nitrate complex. *Langmuir*. **23** (5), 2694-2699 (2007).

[34] Wang M., Xu L., Zhai M., Peng J., Li J., Wei G., γ-ray radiation-induced synthesis and Fe (III) ion adsorption of carboxymethylated chitosan hydrogels. *Carbohydrate polymers*. **74**(3), 498-503 (2008)

[35] Somsook E., Hinsin D., Buakhrong P., Teanchai R., Mophan N., Pohmakotr M., et al., Interactions between iron (III) and sucrose, dextran, or starch in complexes. *Carbohydrate polymers*. **61** (3):281-287 (2005).

[36] Reetz M.T., Helbig W., Size-selective synthesis of nanostructured transition metal clusters. *Journal of the American Chemical Society*. **116**(16), 7401-7402 (1994).

[37] Ramimoghadam D., Bagheri, S., Abd Hamid, S.B., Progress in electrochemical synthesis of magnetic iron oxide nanoparticles. *Journal of Magnetism and Magnetic Materials*. 368, 207-229 (2014).

[38] Aghazadeh M., Karimzadeh I., Ganjali M.R., Electrochemical evaluation of the performance of cathodically grown ultra-fine magnetite nanoparticles as electrode material for supercapacitor applications. *Journal of Materials Science: Materials in Electronics*. **28**(18), 13532-13539 (2017).

[39] De Queiroz A.A., Soares D.A., Trzesniak P., Abraham G.A., Resistive-type humidity sensors based on PVP–Co and PVP–I_2 complexes. *Journal of Polymer Science Part B: Polymer Physics*. **39**(4),459-469 (2001).

[40] Han M., Yun J., Kim H-I., Lee Y-S., Effect of surface modification of graphene oxide on photochemical stability of poly (vinyl alcohol)/graphene oxide composites. *Journal of Industrial and Engineering Chemistry*. **18**(2), 752-756 (2012).

[41] Yang L., Li Y., Hu H., Jin X., Ye Z., Ma Y., et al., Preparation of novel spherical PVA/ATP composites with macroreticular structure and their adsorption behavior for methylene blue and lead in aqueous solution. *Chemical engineering journal*. 73(2), 446-455 (2011).

[42] Alcântara M., Brant A., Giannini D., Pessoa J., Andrade A., Riella H., et al., Influence of dissolution processing of PVA blends on the characteristics of their hydrogels synthesized by radiation—Part I: Gel fraction, swelling, and mechanical properties. *Radiation Physics and Chemistry*. **81** (9), 1465-1470 (2012).

[43] Gaume J., Rivaton A., Thérias S., Gardette J-L., Influence of nanoclays on the photochemical behaviour of poly (vinyl alcohol). *Polymer degradation and stability*. **97**(4), 488-495 (2012).

[44] Jipa I.M., Stroescu M., Stoica-Guzun A., Dobre T., Jinga S., Zaharescu T., Effect of gamma irradiation on biopolymer composite films of poly (vinyl alcohol) and bacterial cellulose. *Nuclear Instruments and Methods in Physics Research Section B: Beam Interactions with Materials and Atoms*. **278**, 82-87(2012).

[45] Constantin M., Fundueanu G., Bortolotti F., Cortesi R., Ascenzi P., Menegatti E., Preparation and characterisation of poly (vinyl alcohol)/cyclodextrin microspheres as matrix for inclusion and separation of drugs. *International journal of pharmaceutics*. 285(1-2), 87-96 (2004).

[46] Singh R., Kulkarni S., Naik N., Effect of nano sized transition metal salts and metals on thermal decomposition behavior of polyvinyl alcohol. *Adv Mater Lett*. **4**, 82-88, (2013).

[47] Ahmed M., Hamid M.A., Sarhan A., Ali A., Synthesis and Structural Characterization of Polypyrrole (PPy)-Chitosan (Cs) Nanocomposite: Influence of UV Irradiation. *Global Journal of Physics*, **7** (1), 2018.

[48] Sarhan A., Preparation and Structure of Silver-Nanoparticles Stabilized with Poly (vinyl alcohol) by electrochemical method for antimicrobial application. *Global Journal of Physics*. 2018;8(1):765-77.

[49] Tauc J., Optical properties of amorphous semiconductors. Amorphous and liquid semiconductors. *Springer*, 159-220(1974).

[50] Chand P., Gaur A., Kumar A., Structural and optical properties of ZnO nanoparticles synthesized at different pH values. *Journal of alloys and compounds*, **539**, 174-178 (2012).

[51] Abdelrazek E, Elashmawi I, Labeeb S. Chitosan filler effects on the experimental characterization, spectroscopic investigation and thermal studies of PVA/PVP blend films. Physica B: Condensed Matter. 2010;405(8):2021-7.

[52] Morsi M., Oraby A., Elshahawy A., El-Hady R.A., Preparation, structural analysis, morphological investigation and electrical properties of gold nanoparticles filled polyvinyl alcohol/carboxymethyl cellulose blend. *Journal of Materials Research and Technology*. **8**(6), 5996-6010 (2019).

[53] Laot C.M., Marand E., Oyama H.T., Spectroscopic characterization of molecular interdiffusion at a poly (vinyl pyrrolidone)/vinyl ester interface. *Polymer*, 40(5), 1095-1108 (1999).

[54] Li X, Goh S, Lai Y, Wee A. Miscibility of carboxyl-containing polysiloxane/poly (vinylpyridine) blends. *Polymer*. **41** (17), 6563-6571 (2000).

[55] Fahmy T., Sarhan A., Elsayed I., Ahmed M., Effect of UV irradiation on the structure and optical properties of PVA/$CuCl_2$. *Journal of Advances in Physics*. 14 (2), 2018.

[56] Su Y., Wu, Y., Liu, M., Qing, Y., Zhou, J., & Wu, Y., Ferric Ions Modified Polyvinyl Alcohol for Enhanced Molecular Structure and Mechanical Performance., *Int J Pharm Pharm Sci*, 13(6), 1412.

[57] Ahmed M., Abd-Elhamid M., Sarhan A., Hassan A., Characteristic and thermal stimulated depolarization current of poly (vinyl chloride-co-vinyl acetate-co-2-hydroxy propyl acrylate) Zn onanocomposite. *Global Journal of Physics*., **5(**2), 585-594 (2017)

[58] Polu A.R, Kumar R., Preparation and characterization of pva based solid polymer electrolytes for electrochemical cell applications. *Chinese Journal of Polymer Science*. **31**(4), 641-648 (2013).

[59] Kawashima Y., Yamamoto H., Takeuchi H., Kuno Y., Mucoadhesive DL-lactide/glycolide copolymer nanospheres coated with chitosan to improve oral delivery of elcatonin. *Pharmaceutical development and technology*. **5** (1), 77-85 (2005).

[60] des Rieux A., Fievez V., Garinot M., Schneider Y-J, Préat V., Nanoparticles as potential oral delivery systems of proteins and vaccines: a mechanistic approach. *Journal of controlled release*. **116** (1), 1-27 (2006).

[61] Ansari S.A., Oves M., Satar R., Khan A., Ahmad S.I., Jafri M.A., et al., Antibacterial activity of iron oxide nanoparticles synthesized by co-precipitation technology against Bacillus cereus and Klebsiella pneumoniae. *Polish Journal of Chemical Technology*. **19** (4), 110 (2017).

[62] Ali A.A., Elmahdy M.M., Sarhan A., Abdel Hamid M.I., Ahmed M.T., Structure and dynamics of polypyrrole/chitosan nanocomposites. *Polymer International*. **67**(12), 1615-1628 (2018).